Evolution of silver in a eutectic-based Bi2O3–Ag metamaterial

K. Sadecka, Marie-Hélène Berger, K. Orlinski, I. Jozwik, D. A. Pawlak

HAL Id: hal-01504431

https://minesparis-psl.hal.science/hal-01504431

Submitted on 1 Aug 2018

Eutectics

CrossMark

Evolution of silver in a eutectic-based Bi$_2$O$_3$–Ag metamaterial

K. Sadecka[1,*], M. H. Berger[2], K. Orlinski[1], I. Jozwik[1], and D. A. Pawlak[1,3]

[1] *Institute of Electronic Materials Technology, Wólczyńska 133, 01-919 Warsaw, Poland*
[2] *MINES ParisTech, MAT - Centre des matériaux, CNRS UMR 7633, PSL Research University, BP 87, 91003 Évry, France*
[3] *Centre of New Technologies, University of Warsaw, ul. Banacha 2C, 02-097 Warsaw, Poland*

ABSTRACT

The development of novel manufacturing techniques of nano-/micromaterials, especially metallodielectric materials, has enabled dynamic development of such fields as nanoplasmonics. However, the fabrication methods are still mostly based on time-consuming and costly top-down techniques limited to two-dimensional materials. Recently, directional solidification has been proposed and utilized for manufacturing of volumetric nanoplasmonic materials using the example of a Bi$_2$O$_3$–Ag eutectic-based nanocomposite. Here, we explain the evolution of silver in this composite, from the crystal growth through the post-growth annealing processes. Investigation with tunneling electron microscopy shows that silver initially enters the composite as an amorphous AgBiO$_3$ phase, which is formed as a wetting layer between the grains of Bi$_2$O$_3$ primary phase. The post-growth annealing leads to decomposition of the amorphous phase into Bi$_2$O$_3$ nanocrystals and intergranular Ag nanoparticles, providing the tunable localized surface plasmon resonance at yellow light wavelengths.

Introduction

Plasmonics [1, 2] is currently one of the rapidly developing fields due to its role in enhancing optical properties, which makes it useful for application in solar cell efficiency enhancement [3, 4], cancer treatment [5], improved hard disks [6], lasers [7] and home-used diagnostics [8]. To achieve plasmonic effects on local field enhancement, localized surface plasmon resonance (LSPR) or surface plasmon propagation, an interface between two media—plasmonic (metallic-like) and dielectric—is needed [9]. Due to the collective oscillations of free charges, which are responsible for negative real permittivity, metals like silver and gold are currently the most used materials in plasmonics [10]. However, though other plasmonic materials have been considered [11, 12], it is still silver in the visible wavelengths, which is most widely used due to its lowest optical losses [13] and highest electrical conductivity at room temperature [14].

Address correspondence to E-mail: katarzyna.sadecka@itme.edu.pl

Springer

Recently, eutectic solidification [15, 16] has been proposed as one of the most promising bottom-up methods for manufacturing of metamaterials [17–20], plasmonic materials [21, 22] and photonic crystals [23, 24]. Eutectic solidification enables crystallization of a two-phase solid, often with an interesting self-organized micro-/nanostructure (typical are rod-like and lamellar structures) from a miscible liquid phase at a certain temperature [25]. Eutectic composites have been investigated for various applications such as solar energy conversion [26–28], power generation gas turbines [29], scintillators [30, 31] or second-harmonic generators [32]. The plasmonic effect was presented in a eutectic composite for the first time with a Bi_2O_3–Ag composite [21, 22]. After annealing the Bi_2O_3–Ag eutectic material, metal nanoparticles (silver and bismuth) are formed, which are responsible for the occurrence of plasmonic resonance in the visible wavelength range, at ∼595 nm. Using different annealing conditions such as the atmosphere, time and temperature, it is possible to control the peak frequency of the LSPR [22]. However, the development of metallic silver in this material is not yet well understood. Here, we demonstrate the evolution of silver in a Bi_2O_3–Ag eutectic starting from the crystal growth, and formation of the microstructure, through the influence of the post-growth annealing of the samples on its micro-/nanostructure and thus the optical properties. The analysis is based on high-resolution transmission electron microscopy (HRTEM) and selected area diffraction (SAD).

Materials and methods

The Bi_2O_3–Ag material was obtained by the micro-pulling down method [33, 34] in a nitrogen atmosphere from pure powders of bismuth oxide (Alfa Aesar, 99.99% purity) and silver (Alfa Aesar, 99.95% purity). Detailed growth and preparation methods have been described elsewhere [21]. After growth, the samples were annealed in vacuum at 600 °C for 60 min [22]. The obtained Bi_2O_3–Ag composites were characterized by the following methods: high-resolution transmission electron microscopy (HRTEM) connected with selected area electron diffraction and with scanning transmission electron microscopy (STEM) with energy-dispersive X-ray spectroscopy (EDX). Samples for transmission electron microscope analysis were prepared by a focused ion beam (FIB)

lift-out technique using a 30-keV Ga+ ion beam in an AURIGA CrossBeam Workstation (Carl Zeiss) equipped with a Canion FIB column (Orsay Physics). TEM investigations were conducted with the use of a Tecnai F20ST (FEI) TEM-STEM microscope with field emission gun and electron beam energy of 200 keV and coupled to a high-angle annular detector (HAADF) and a EDAX X-ray energy-dispersive spectrometer (EDX). The software "TE Imaging & Analysis" (EI) was used to provide standardless semiquantitative analyses of the EDX spectra. These analyses take into account the thickness and the chemical elements of the thin foil (ZAF corrections) and use preregistered K factors. Differential scanning calorimetry/thermogravimetry (DSC/TG) measurements were taken on an STA 449 (NETZSCH) with a platinum furnace under argon flow with different amounts of purge oxygen. Stoichiometric portions of powders were measured out and mixed manually with minor addition of isopropyl alcohol until a homogeneous color was achieved. The mixture was subsequently dried at 80 °C to remove the alcohol. The signals were measured with a Pt–Rh thermocouple using platinum crucibles in a temperature range from room temperature to 1173 K with a heating/cooling rate of 10 K min^{-1}. Bi_2O_3–Ag powder mixtures were heated to 1173 K and cooled to 923 K. The process was repeated three times in each atmosphere to ensure homogeneity of the melt. The solidus temperatures were extracted from the heating curves as onset values, whereas liquidus temperatures were extracted from the cooling curves as the end temperatures. The influence of oxygen content on the phase diagram was investigated using powder samples of mixed bismuth oxide (99.9% purity) with silver (99.95% purity) in the range of 0–10 mol% in steps of 1 mol%.

Results and discussion

From the Ag–½(Bi_2O_3) phase diagram [35] in the mentioned system, several transformations at an oxygen partial pressure of 1.01×10^5 Pa are observed (1) allotropic of Bi_2O_3, α-$Bi_2O_3 \rightarrow \delta$-$Bi_2O_3$), (2) monotectic (Ag) + Liq2 ↔ Liq1 at 939 °C and eutectic reaction (Ag) + α-Bi_2O_3 ↔ Liq2 at 687 °C with a composition of 18.54 mol% Ag and 81.46 mol% $^1/_2Bi_2O_3$ (∼8.6 vol% Ag). With the decrease in oxygen content in the atmosphere, the composition of the

eutectic point shifts toward lower content of silver (12.3 mol% Ag for $pO_2 = 2.1 \times 10^4$ Pa, ~5.5 vol% Ag). In our growth experiments, the successful composition that led to good-quality Bi_2O_3–Ag rods was 15.4 mol% Ag and 84.5 mol% $^1/_2Bi_2O_3$ (~7.8 vol% Ag). This composition is between the eutectic points determined by Assal et al. [35] for different oxygen partial pressures, as shown in Fig. 1. We have confirmed part of the phase diagrams investigated by Assal et al. with DSC/TG measurements for different partial pressures of oxygen: $pO_2 = 0.32 \times 10^4$, 0.77×10^4, 1.43×10^4 and 2×10^4 Pa. It can be noticed that the liquidus line is in a very good agreement; however, the solidus line yielded a slightly lower temperature.

The as-grown Bi_2O_3–Ag composite is characterized by a three-dimensional micro-/nanostructure of silver-containing phase in a Bi_2O_3 matrix. Silver is located in a second phase wetting the Bi_2O_3 grain boundaries and at triple points where it adopts a triangular shape. Between two Bi_2O_3 grains, silver is in the form of plates with lengths of several tens of microns and thicknesses of a few nanometers.

To investigate the phase in which silver is placed in the Bi_2O_3–Ag composite during growth and to understand the processes which lead to the formation of silver nanoparticles after the annealing of the material, high-resolution transmission electron microscopy has been performed on the as-grown and annealed-in-vacuum samples. Both the selected area electron diffraction and the energy-dispersive X-ray spectroscopy confirmed that the as-grown material consists of two phases. In the region analyzed, the dominant phase is γ-Bi_2O_3 (bcc, $a = 1.027$ nm), which was detected in the larger grains. These grains enclosed smaller grains, which were probably the α-Bi_2O_3 phase. However, the second phase previously not recognized by other techniques is an amorphous (halo in the SAD pattern) phase containing Bi, Ag and O, with an atomic ratio Bi/Ag $\approx$ 1, as shown in Fig. 2. The shape of this second phase, forming triangles at Bi_2O_3 triple points and wetting the Bi_2O_3 grain boundaries, is consistent with the solidification of a liquid after the crystallization of the major primary phase, in this case Bi_2O_3. The radius of the halo in Fig. 2e provides the distance of the first neighbors in the amorphous phase, which is 0.32 nm (superimposed with the $d_{310} = 0.325$ nm of γ-Bi_2O_3). This distance does not match with the strongest reflections of silver or silver oxides but with the strongest reflections of γ-Bi_2O_3 as well as with those of an ilmenite-type, $AgBiO_3$ phase [36]. The amorphous phase might enclose clusters of atoms prefiguring an ilmenite crystal. Ilmenite-type oxides have two kinds of combinations of metal cations: $A^{2+}M^{4+}O_3$ and $A^+M^{5+}O_3$ [37], where $AgBiO_3$ corresponds to the second one.

Due to a strong dependence of the eutectic point on the content of oxygen in the atmosphere, it is not
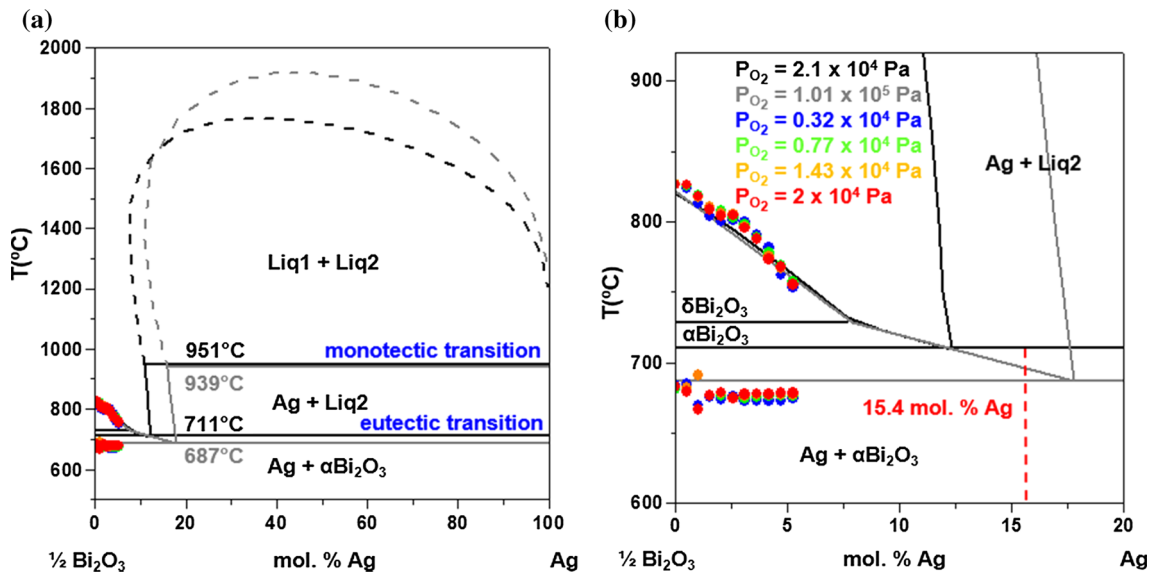
Figure 1 Eutectic phase diagram of Bi_2O_3–Ag system. Adapted with permission from Wiley. Liquidus and solidus curves (*dots*) for Bi_2O_3–Ag mixtures measured in atmospheres with different oxygen contents. The material investigated in this paper was grown from 15.4 mol% of Ag and 84.6 mol% of $^1/_2Bi_2O_3$.
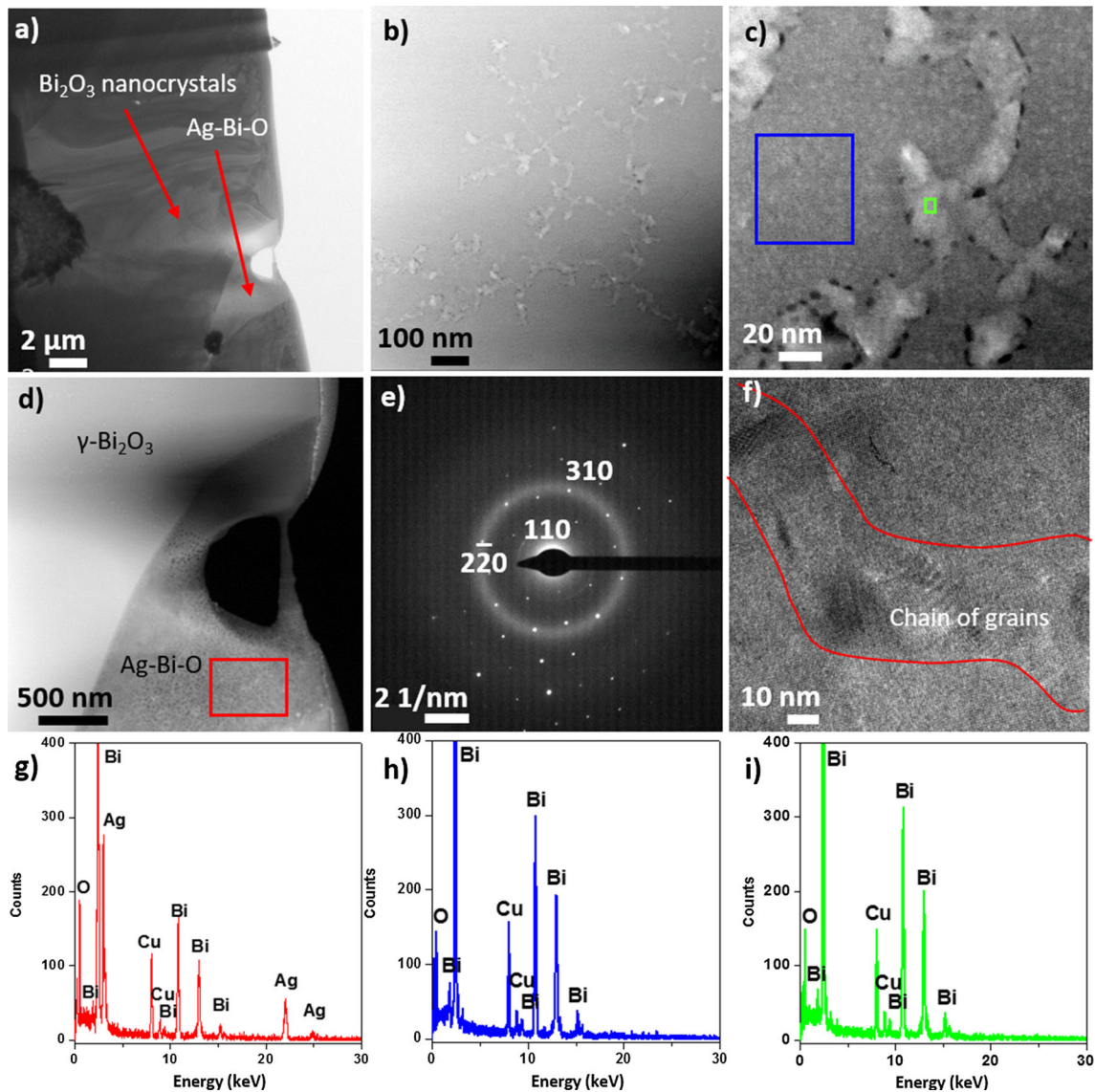
Figure 2 Structural analysis of the as-grown Bi_2O_3–Ag eutectic material. **a** Bright-field image of the entire FIB cut of the sample with selected phases. **b, c** STEM-HAADF images of chains of Bi_2O_3 nanocrystals within the γ-Bi_2O_3 matrix, potentially also γ-Bi_2O_3. The γ-Bi_2O_3 larger grain encloses chains of smaller α-Bi_2O_3 grains. **d** STEM-HAADF image and **e** SAD pattern across Bi_2O_3- and Ag-based phase. Spots corresponding to the γ-Bi_2O_3 are in [001] zone axis. The halo is formed by the second phase and is typical of an amorphous phase. **f** Chain of probable α-Bi_2O_3 grains within bigger grains of γ-Bi_2O_3. EDX spectrum of **g** the $AgBiO_3$ phase, **h** γ-Bi_2O_3 matrix and **i** Bi_2O_3 larger grains.

clear whether the composition of the Bi_2O_3–Ag composite we have grown is shifted to a higher abundance of Bi_2O_3 or Ag, as shown in Fig. 1. From the phase diagram of Bi_2O_3–Ag [35], if the composition is shifted from the eutectic point to a higher abundance of Bi_2O_3, it is the Bi_2O_3 phase that should crystallize first in contact with a liquid phase. While, if the composition is shifted toward a higher abundance of Ag, the Ag phase should crystallize first, and then, the eutectic will be made of Bi_2O_3 and Ag.

The geometry of the Ag–Bi–O phase placed in between the grains of Bi_2O_3 is typical of a liquid phase that solidified after the main grains, though potentially it could be a Ag-containing phase in which the grains were squeezed by growing Bi_2O_3 grains. The $AgBiO_3$ phase is probably formed in the following reactions [38]: $4AgO + Bi_2O_3 \rightarrow 2AgBiO_3 + Ag_2O$, and $Ag_2O + Bi_2O_3 \rightarrow 2AgBiO_2$.

The amorphous Ag–Bi–O phase is not stable when irradiated by the electron beam and partially

decomposes into ca. 50-nm-diameter γ-Bi_2O_3 nanocrystallites and metallic silver particles a few nanometers in size. Nanocrystals of bismuth oxide up to 50 nm in size are clearly seen in the dark-field image (Fig. 3a) and as bright spots at the SAD image (Fig. 3b). The first internal ring is from the amorphous Ag–Bi–O phase. A second finer halo at 0.23 nm is clearly observed, which may correspond to metallic nanosilver (strongest reflection 111 Ag fcc) exsoluted from the Ag–Bi–O phase, with sizes of a few nm, as shown in Fig. 3b.

Concerning the optical properties of the Bi_2O_3–Ag composite, it has been previously confirmed that only the annealed samples demonstrate LSPR, due to the formation of Ag nanoparticles after the post-growth annealing [21]. The best of the investigated annealing conditions, which led to the most intensive LSPR peak, was annealing at 600 °C for 60 min in vacuum [22]. That is why such samples were investigated here further, as shown in Fig. 4. In the vacuum-annealed samples in comparison with the as-grown (un-annealed) samples, it can be seen that the large Bi_2O_3 grains did not change, while the amorphous phase transformed during the annealing into γ-Bi_2O_3 grains several hundreds of nm in size, as shown in Fig. 4a–c, and intergranular precipitates of Ag a few nm in size (Fig. 4d, red circle), as confirmed by EDX.

Both the annealing and irradiation with the electron beam during the TEM experiments resulted in phase and structural change of the material, which can be the result of a few processes. Thermal stability studies of $AgBiO_3$ [39] performed in argon show weight loss from $AgBiO_3$, which corresponds to two transitions such as:

$$AgBiO_3 \xrightarrow{250-280\,°C} AgBiO_2 \xrightarrow{300-550\,°C} Ag + Bi$$

As a result of the final decomposition of $AgBiO_3$, a mixture of metallic silver and bismuth can be obtained. The formation of both Ag and Bi nanoparticles was already previously observed by us in this material [22]. This suggests that it is the decomposition of $AgBiO_3$ into Ag and Bi nanoparticles in between the big Bi_2O_3 grains, which probably causes the formation of the smaller (ca. few hundred nanometers in size) Bi_2O_3 grains. The few-hundred-nm-in-size Bi_2O_3 grains have grown from the nano-Bi_2O_3 grains seen in Fig. 3a, with decomposition of the amorphous phase. In Fig. 5, we illustrate the proposed mechanism of silver evolution in the Bi_2O_3–Ag system.

Conclusions

In summary, an explanation of the evolution of silver in a Bi_2O_3–Ag eutectic composite from the crystal growth through the post-growth annealing processes has been presented. In the as-grown samples, silver is inserted in an amorphous phase enclosing $AgBiO_3$ clusters, which is formed as intergranular films and triple points wetting the grains of Bi_2O_3 primary phase. After the post-growth annealing, the $AgBiO_3$ phase decomposes into Bi_2O_3 nanocrystals and intergranular Ag. These studies give us an explanation for the origin of silver nanoparticles in the Bi_2O_3–Ag eutectic-based material after the annealing procedure and thus the localized surface plasmon resonance at yellow light wavelengths.
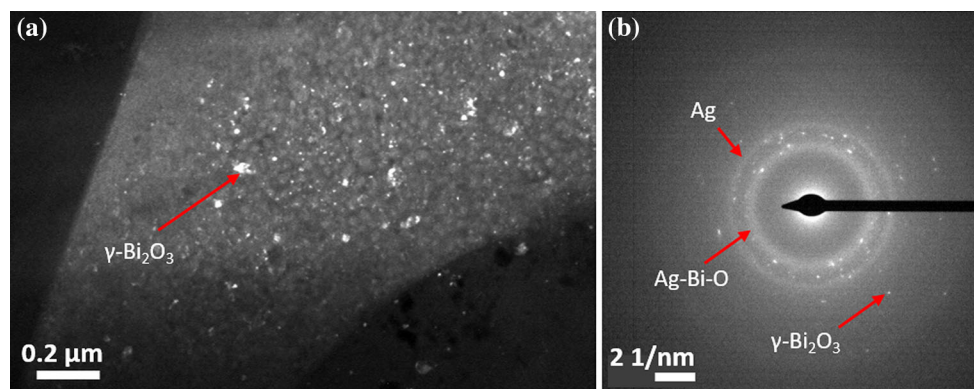
**Figure 3** Decomposition of the amorphous $AgBiO_3$ phase under electron beam irradiation into nanocrystalline γ-Bi_2O_3 precipitates and metallic silver to **a** γ-Bi_2O_3 seen as bright grains in the dark-field image and **b** as spots in the indexed SAD. SAD showing the formation of Ag–Bi–O amorphous phase (first smaller ring at 0.32 nm) and nanocrystals of silver (second finer ring at 0.23 nm).
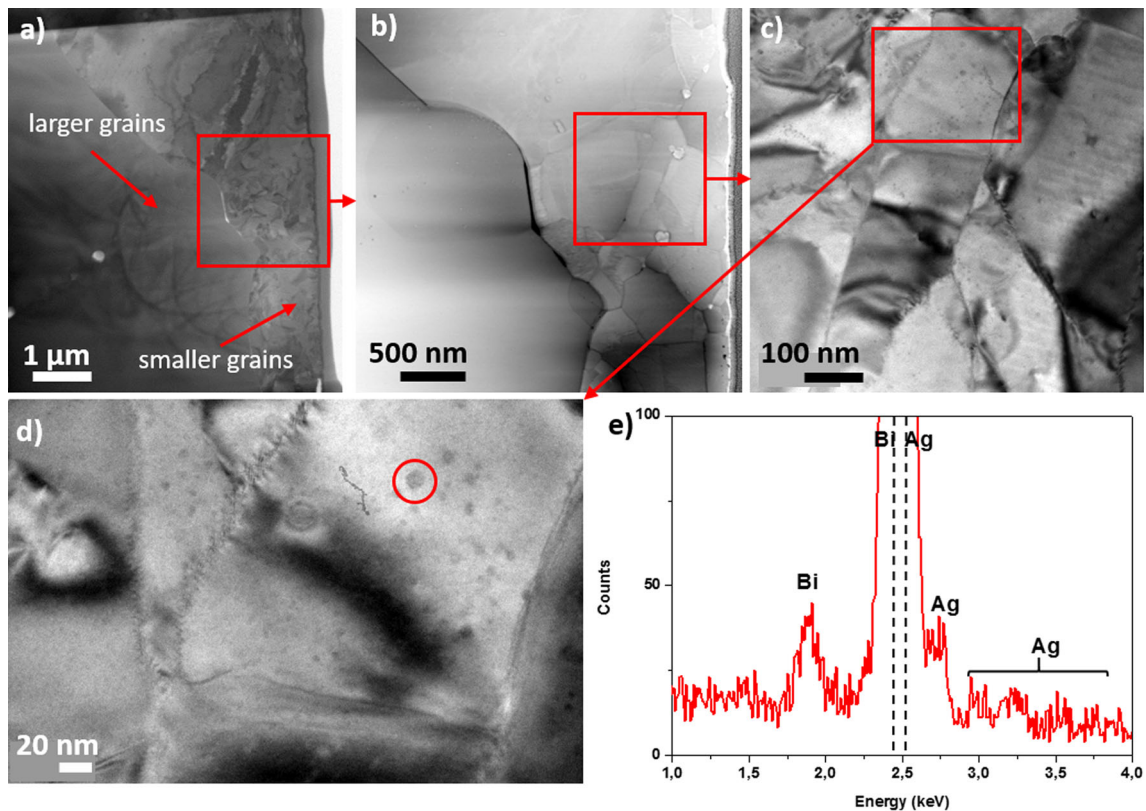
Figure 4 Structural analysis of the annealed-in-vacuum Bi_2O_3–Ag eutectic material. **a**–**c** Progressive zooms by HAADF showing the various scales of the structure with the smaller and larger grains marked, **d**, **e** intergranular precipitates of Ag presented by HAADF with EDX analysis.
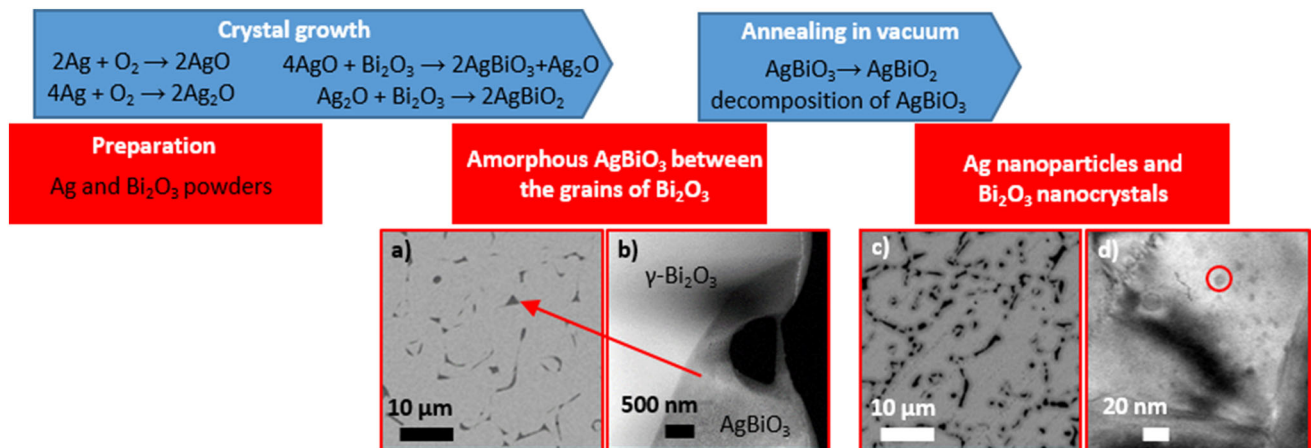
Figure 5 Silver evolution mechanism in Bi_2O_3–Ag system, starting from the crystal growth through the post-growth annealing processes. *Blue arrows* represent processes, *red rectangles*—the resulting micro-/nanostructure. SEM pictures of the microstructures **a** before and **c** after annealing. STEM-HAADF image **b** across Bi_2O_3- and Ag-based phase and **d** intergranular precipitates of Ag.

Acknowledgements

References

[1] Maradudin AA, Sambles JR, Barnes WL (2014) Modern plasmonics. Elsevier, Amsterdam, pp 1–36

[2] Yao K, Liu Y (2014) Plasmonic metamaterials. Nanotechnol Rev 3(2):177–210

[3] Atwater HA, Polman A (2010) Plasmonics for improved photovoltaic devices. Nat Mater 9:205–213

[4] Polman A (2008) Plasmonics applied. Science 322:868–869

[5] Lal S, Clare SE, Halas NJ (2008) Nanoshell-enabled photothermal cancer therapy: impending clinical impact. Acc Chem Res 41:1842–1851

[6] Stipe BC et al (2010) Magnetic recording at 1.5 pb m^{-2} using an integrated plasmonic antenna. Nat Photon 4:484–488

[7] Stockman M (2008) Spasers explained. Nat Photon 2:327–329

[8] Stockman M (2011) Nanoplasmonics: the physics behind the applications. Phys Today 64:39–44

[9] Maier SA (2007) Plasmonics: fundamentals and applications. Springer, Berlin, pp 65–88

[10] West PR et al (2010) Searching for better plasmonic materials. Laser Photon Rev 4:795–808

[11] Naik GV, Shalaev VM, Boltasseva A (2013) Alternative plasmonic materials: beyond gold and silver. Adv Mater 25:3264–3294

[12] Boltasseva A, Atwater H (2011) Low-loss plasmonic metamaterials. Science 331(6015):290–291

[13] Palik ED (1991) Handbook of optical constants of solids. Elsevier Science, Amsterdam, vol 1, 350–356

[14] Serway RA (1998) Principles of physics, 2nd edn. Saunders College Pub, Fort Worth, Texas: London, p 602

[15] Akamatsu S, Plapp M (2016) Eutectic and peritectic solidification patterns. Curr Opin Solid State Mater Sci 20(1):46–54

[16] Rátkai L, Szállás A, Pusztai T, Mohri T, Gránásy L (2015) Ternary eutectic dendrites: pattern formation and scaling properties. J Chem Phys 142:154501–154513

[17] Pawlak DA, Kolodziejak K, Turczynski S, Kisielewski J, Rożniatowski K, Diduszko R, Kaczkan M, Malinowski M (2006) Self-organized, rod-like, micron-scale microstructure of Tb$_3$Sc$_2$Al$_3$O$_{12}$–TbScO$_3$: Pr eutectic. Chem Mater 18(9):2450–2457

[18] Pawlak DA, Turczynski S, Gajc M, Kolodziejak K, Diduszko R, Rozniatowski K, Smalc J, Vendik I (2010) How far are we from making metamaterials by self-organization? The microstructure of highly anisotropic particles with an SRR-like geometry. Adv Funct Mater 20(7):1116–1124

[19] Massaouti M, Basharin AA, Kafesaki M, Acosta MF, Merino RI, Orera VM, Economou EN, Soukoulis CM, Tzortzakis S (2013) Eutectic epsilon-near-zero metamaterial terahertz waveguides. Opt Lett 38:1140–1142

[20] Myroshnychenko V, Stefanski A, Manjavacas A, Kafesaki M, Merino RI, DA OreraVM P, Garcia de Abajo FJ (2012) Interacting plasmon and phonon polaritons in aligned nano- and micro-wires. Opt Express 20:10879–10887

[21] Sadecka K, Gajc M, Orlinski K, Surma HB, Jóźwik-Biała I, Klos A, Sobczak K, Dłużewski P, Toudert J, Pawlak DA (2015) When eutectics meet plasmonics: nanoplasmonic volumetric, self-organized silver-based eutectic. Adv Opt Mater 3(3):381–389

[22] Sadecka K, Toudert J, Surma HB, Pawlak DA (2015) Temperature and atmosphere tunability of the nanoplasmonic resonance of a volumetric eutectic-based Bi$_2$O$_3$–Ag metamaterial. Opt Exp 23(15):19098–19111

[23] Pawlak DA, Lerondel G, Dmytruk I, Kagamitani Y, Durbin S, Fukuda T (2002) Second order self-organized pattern of terbium–scandium–aluminum garnet terbium–scandium perovskite eutectic. J Appl Phys 91(12):9731–9736

[24] Kim J, Aagesen LK, Choi JH, Choi J, Kim HS, Liu J, Cho C, Kang JG, Ramazani A, Thornton K, Braun PV (2015) Template-directed directionally solidified three-dimensionally mesostructured AgCl–KCl eutectic photonic crystals. Adv Mater 27:4551–4559

[25] LLorca J, Orera VM (2006) Directionally solidified eutectic ceramic oxides. Prog Mater Sci 51(6):711–809

[26] Oliete PB, Mesa MC, Merino RI, Orera VM (2016) Directionally solidified Al$_2$O$_3$–Yb$_3$Al$_5$O$_{12}$ eutectics for selective emitters. Sol Energy Mater Sol Cells 144:405–410

[27] Wysmulek K, Sar J, Osewski P, Orlinski K, Kolodziejak K, Trenczek-Zajac A, Radecka M, Pawlak DA (in review) A SrTiO$_3$–TiO$_2$ eutectic composite as a stable photoanode material for photoelectrochemical hydrogen production. Appl. Catalysis B

[28] Kolodziejak K, Sar J, Wysmulek K, Osewski P, Orlinski K, Warczak M, Sadkowski A, Radecka M, Pawlak DA (submitted) When eutectic composites meet photoelectrochemistry—highly stable and efficient UV–visible hybrid photoanodes. Nanoscale

[29] Waku Y, Nakagawa N, Wakamoto T, Ohtsubo H, Shimizu K, Kohtoku Y (1998) High-temperature strength and thermal

stability of a unidirectionally solidified Al2O₃/YAG eutectic composite. J Mater Sci 5:1217–1225. doi:10.1023/A:1004377626345

[30] Yasui N, Ohashi Y, Kobayashi T, Den T (2012) Development of phase-separated scintillators with light-guiding properties. Adv Mater 24:5464–5469

[31] Hishinuma K, Kamada K, Kurosawa S, Yamaji A, Pejchal J, Yokota Y, Ohashi Y, Yoshikawa A (2015) LiF/CaF₂/LiBaF₃ ternary fluoride eutectic scintillator. Jpn J Appl Phys 54(4S):04DH04

[32] Simon F, Clevers S, Gbabode G, Couvrat N, Agasse-Peulon V, Sanselme M, Dupray V, Coquerel G (2015) Enhanced second harmonic generation from an organic self-assembled eutectic binary mixture: a case study with 3-nitrobenzoic and 3,5-dinitrobenzoic acids. Cryst Growth Des 15(2):946–960

[33] Fukuda T, Rudolph P, Uda S (2004) Fiber crystal growth from melt. Springer-Verlag Berlin Heidelberg, New York, pp 1–46

[34] Fukuda T, Chani VI (2007) Shaped crystals growth by micro-pulling-down technique. Springer-Verlag Berlin Heidelberg, New York, pp 3–36

[35] Assal J et al (1999) Experimental phase diagram study and thermodynamic optimization of the Ag–Bi–O system. J Am Ceram Soc 82(3):711–715

[36] Kumada N (2000) Neutron powder diffraction refinement of ilmenite-type bismuth oxides: ABiO₃ (A = Na, Ag). Mater Res Bull 35(14):2397–2402

[37] Wells AF (1975) Structural inorganic chemistry, 4th edn. Claredon Press, Oxford, p 479

[38] Passaniti et al (1995) United States Patent, Patent Number: 5,389,469. Date of Patent: 14 Feb 1995

[39] Sharma R (2004) Characterization of AgBiO₃ with the cubic KSbO₃ structure. Indian J Chem Sect 43A(1):11–17